*Research Article*

# Finite Element Least Square Technique for Newtonian Fluid Flow through a Semicircular Cylinder of Recirculating Region via COMSOL Multiphysics

**Ilyas Khan** [ID],[1] **Abid A. Memon,**[2] **M. Asif Memon,**[2] **Kaleemullah Bhatti,**[2] **Gul M. Shaikh,**[2] **Dumitru Baleanu** [ID],[3,4,5] **and Ziyad A. Alhussain**[1]

[1]*Department of Mathematics, College of Science Al-Zulfi, Majmaah University, Al-Majmaah 11952, Saudi Arabia*
[2]*Department of Mathematics, Sukkur IBA University, Sukkur, Sindh, Pakistan*
[3]*Department of Mathematics, Cankaya University, Ankara 06790, Turkey*
[4]*Institute of Space Sciences, Magurele 077125, Romania*
[5]*Department of Medical Research, China Medical University Hospital, China Medical University, Taichung 40447, Taiwan*

Correspondence should be addressed to Ilyas Khan; i.said@mu.edu.sa and Dumitru Baleanu; baleanu@mail.cmuh.org.tw

This article aims to study Newtonian fluid flow modeling and simulation through a rectangular channel embedded in a semicircular cylinder with the range of Reynolds number from 100 to 1500. The fluid is considered as laminar and Newtonian, and the problem is time independent. A numerical procedure of finite element's least Square technique is implemented through COMSOL multiphysics 5.4. The problem is validated through asymptotic solution governed through the screen boundary condition. The vortex length of the recirculating region formed at the back of the cylinder and orientation of velocity field and pressure will be discussed by three horizontal and four vertical lines along the recirculating region in terms of Reynolds number. It was found that the two vortices of unequal size have appeared and the lengths of these vortices are increased with the increase Reynolds number. Also, the empirical equations through the linear regression procedure were determined for those vortices. The orientation of the velocity magnitude as well as pressure along the lines passing through the center of upper and lower vortices are the same.

## 1. Introduction

In the engineering sciences, the Navier–Stokes equations governed through Newton's law of motion possess the paramount importance and describe the physical phenomenon of flow in the form of nonlinear partial differential equations in the vector form. They help to model so many physical problems such as blood flow in the human or animal body, manufacturing designs, manufacturing car, and aircraft designs, calculating drag force of air flow around wings, removal of pollutions, weather conditions, rivers, flow of oceans, etc.

The literature studies reveal that when the fluid enters the region within a sufficient velocity magnitude and comes into contact with the bluff bodies of any shape, the formation of vortex shedding and recirculating flow is taken place at the back of the observed body. The size of this recirculating region or increasing with the increase in the velocity magnitude by which the fluid comes into the strike with these bluff bodies. These vortices are attached as well as detached periodically and creating a von Karman vortex region. The fluid which passes through the bodies created the vortices with the negative pressure, which means that, any object presented in the region might be attracted by these vortices. With the range of ratios 1.6 to 4 to the height of the rectangular channel with a diameter of the circle and ranging up to 5 the Stuart number, the vortex structure and its increment was studied by Rashid et al. [1]. It was derived that

the formation of the recirculation region or vortex takes place in the back of circular obstacles when the fluid flows in the influence of the magnetic field. Moreover, to keep the drag force lower, a critical Stuart number was discussed. With the multigrid acceleration technique in the numerical finite volume method, the fluid flow through the lid-driven cavity which included a circular cylinder was observed by Faycal et al. [2]. The study was laminar and Newtonian and analyzed with the lower to high Reynolds number up to 1500. It was deduced that the formation of the recirculating region appeared at the back of the circular cylinder and length is directly proportional with the Reynolds number. An investigation of the heat transfer in the rectangular channel with circular obstacle and the fluid flow was discussed with the use of finite volume procedure using the Reynolds number from 50 to 180. Gholani and Dheman [3] found that the frequency of vortex production along the circular bluff, lift force, and drag force was showing the positive response with increasing nondimensional Reynolds number. A unified finite element technique of Galerkin's scheme of least square to deal with all types of compressible and incompressible fluid flows was suggested by Hauke and Haughes [4]. According to their findings if the Navier–Stokes equation can be represented as quasi-linear form with the pressure, velocity, and temperature as entropy variables, then a combined formulation of discretization can be derived to solve the fluid flow problems. An asymptotic solution was given by Elder [5] for the streamwise velocity at the outlet of the rectangular channel and placing a solid screen at the middle of the channel at an angle $\theta$. The relationship was good enough to understand the behavior of flow before and after the screen. Memon et al. [6], with the help of comsol multiphysics 5.4, carried out graphical modeling for the fluid flow via the channel imposed with three screens at angles from–45° to 45° and at unit distance from each other. They found that drag force is reduced by turning screens from 0 to 45° when moving in counter-clockwise direction and also the process becomes faster by adding more screens. Memon et al. [7] presented a pattern of fluid flow behavior through the screens with the use of different resistance coefficient for the screens and described that the optimum velocity, as well as pressure at the exit of the channel will be optimized by increasing the resistance in the screens. The problem was solved through the FEM package COMSOL multiphysics 5.4. Therefore, different researchers [8–11] put their efforts to describe the fluid flows through circular bluffs fixing at in the channel. By considering an unspecified Couette flow, the equation of motion of second grade fluid were worked out with the shift of variables followed by the finite integral transform with the slip and no-slip boundary states [12]. They found that, for the slip flow, an alternative variation of the velocity very near the wall has been seen, which was quite a different behavior for the slip condition. An investigation [13] was done for the oscillation mode created by solving Burger's equation for a porous medium surrounded by the circular tube with the little boost of Fourier series which generated the time-dependent trapezoidal pressure gradient. It was revealed with the simulation that, for all kind of Burger's fluid, the drag forces at the wall are decreasing with the increase in porosity that also resulted with the increase in velocity. Later, it was Fomicheva et al. [14] who worked Thomas algorithm of implicit finite difference scheme over micropolar fluidic nature and the funnel flow followed by Navier–Stokes equations. The study contributed the velocity and pressure distribution for the fully coupled flow in the micropolar fluidic medium. The two articles [15, 16] on the oscillatory behavior (Kamenev-type and Philos-type oscillation Criteria) and asymptotic behavior of the fluid were published and that based on working on the higher order differential equations with some additional terms. The criteria explained in the articles were also illustrated with the benchmark examples.

The article aims to observe the steady and Newtonian fluid flow through the rectangular channel fitted with a semicircular cylinder. The fluid behavior was predicted with ranging the Reynolds number from 100 to 1500. The simulation was obtained with COMSOL multiphysics 5.4. Firstly, we will try to validate our results with the asymptotic solution for the streamwise velocity at the outlet of the channel by fitting a solid screen at the middle of the channel including semicylinder and then without semicylinder. The vortex lengths formed at the back of the semicylinder is discussed with graphs in terms of the Reynolds number. The orientation of the velocity field and pressure along the three horizontal lines and four vertical lines on the recirculation region will be discussed.

*1.1. Channel Description and Meshing.* Here, we choose the geometry to check the fluid flow around the vortex formed around the semicircle. Figure 1 is showing the structure of the channel. The channel is composed of two parallel plates of length 4 m each, and a semicircle of radius 0.2 m is placed near but not so much near the inlet. To analyze the laminar and Newtonian fluid with the property of fixed volume or incompressibility through the channel it is traditional to use the Reynolds number. The airflow is allowed to enter from the left entrance of the channel with $U_{in}$ depending on the Reynolds number. The channel is open from right-hand side and the pressure is taken zero there with the condition that no back fluid flow will be allowed. The upper and lower boundaries of the channel formed by two parallel plates are recognized as walls with slip conditions applying on them in order to observe zero viscous near the boundary.

Robust finite element technique of least Square Galerkin's scheme has been employed to achieve numerical approximation for the velocity field, as well as pressure. It is the beauty of all schemes depending on approximation to divide the whole domain into subdomains called elements. The chosen domain is divided by irregular triangular elements about 2886 with quality 0.64 as minimum and 0.945 with average quality, as shown in Figure 2. The quality we mean is the percentage of approximation from a single element.

*1.2. Governing Equations and Boundaries.* The governing second-order PDEs derived with the conservative law of
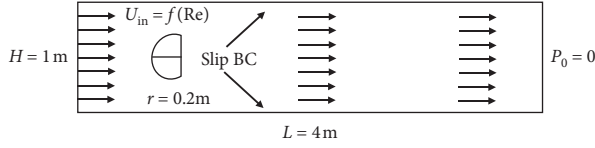
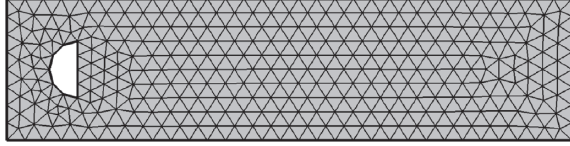Figure 1: Geometrical description of the channel.



Figure 2: View of the coarse mesh of the geometry.

momentum (1) and mass (2) with steady-state (3) are considered to create a simulation of the fluid behavior while air is striking with the semicircular cylinder fixed between the parallel plates:

$$\frac{\partial \vec{V}}{\partial t} + (\vec{V} \cdot t\nabla)\vec{V} = -\frac{1}{\rho}\nabla p + \mu\nabla^2\vec{V} + F, \tag{1}$$

$$\nabla \cdot \vec{V} = 0, \tag{2}$$

$$\frac{\partial \vec{V}}{\partial t} = 0, \tag{3}$$

where $V = <u, v>$ are the velocity of the fluid with horizontal and vertical components $u$ and $v$, respectively, and $\mu$ and $\rho$ are the viscosity and density at the temperature $T = 20°$. As the fluid is allowed to enter with not any source, therefore $F = 0$. The behavior of the flow is testing at the region where the vortex is formed, and we call it the recirculating region in the article and described it through the nondimensional and obviously a traditional number, Reynolds number, which is described by equation (4):

$$\text{Re} = \frac{\rho U_{\text{in}} L}{\mu}. \tag{4}$$

where $L$ is the length of the channel and $U_{\text{in}}$ is the average velocity which becomes the source for the fluid to enter in the channel. The study has been carried out to apply the slip boundary conditions (5)–(7) which means the velocity along the upper and lower walls are not zero. Let $n$ be the vector normal to the velocity; then, slip boundary conditions are defined as equations

$$\vec{V} \cdot \vec{n} = 0, \tag{5}$$

$$\vec{K} - (\vec{K} \cdot t\vec{n})\vec{n} = 0, \tag{6}$$

where

$$\vec{K} = \nu\left(\nabla\vec{V} + (\nabla\vec{V})^T\right)\vec{n}. \tag{7}$$

We are getting help using the screen boundary condition by considering refraction coefficient $\eta$ of 0.78 and resistance

coefficient $\kappa$ of 2.2. First, we calculate the streamwise velocity at the outlet by using only screen attached at the middle with inclination of 45° and with both the semicircular cylinder and screen. The results show the good agreement with the asymptotic solution. Let the + sign show the velocity orientation before upstream and − sign show the velocity downstream; then, we can determine the screen boundary condition and asymptotic solution by (8)–(10) and (11), respectively:

$$[\rho\vec{V} \cdot \vec{n}]_-^+ = 0, \tag{8}$$

$$\left[\rho - \vec{(n)}^T K\vec{n} + \rho(\vec{V} \times t\vec{n})^2\right]_-^+ = -\frac{k}{2}\rho_-\left(\vec{V_-} \times t\vec{n}\right)^2, \tag{9}$$

$$\vec{n} \times \vec{V}_+ = \eta\left(\vec{n} \times t\vec{V_-}\right). \tag{10}$$

The system of PDEs on behalf of these boundary conditions will be solved through COMSOL multiphysics 5.4 with Galerkin's Scheme of Least Square [4]:

$$\frac{((u/U_{\text{in}}) - 1)(1 + \eta + \kappa\cos^2\theta)}{(1 - \eta)\tan\theta\kappa\cos^2\theta} = \frac{2}{\pi}\log\left(\cot\left(\frac{\pi y}{2}\right)\right), \tag{11}$$

*1.3. Validation and Comparison.* The results obtained through the COMSOL multiphysics 5.4 are compared with the analytic solution. For the purpose, we solved the problem first by placing a semicylinder and a solid wire gauze in front of it to obtain the streamwise velocity given by equation (11). And then, we solved the same problem without the cylinder and with only solid wire gauze. Figures 3(a) and 3(b) are depicted and are showing how good the results are related to each other. The results satisfy us and we move our research forward.

## 2. Results and Discussion

*2.1. Streamline Presentation of the Velocity Field and Vortex Lengths.* In Figure 4, the velocity field through the streamlines influences the Reynolds number. We see at Re = 100, in Figure 4(a), the two vortices appeared at the back of a circular cylinder. In the paper, we call upper vortex as primary vortex and the lower vortex is the secondary vortex. Initially, the length of the primary vortex appears a little bit less than the secondary vortex. As the Reynolds number is growing, the lengths of the secondary as well as the primary are increasing and comparable with each other. We might look at the vortex forming at Re = 300 and 600 in Figure 4(b) and 4(c), where the primary vortex appeared greater than secondary vortex. At Re = 900 in Figure 4(d), we can also see that the secondary vortex is appearing bigger in length.

The lengths of these two vortices are influenced by the increasing Reynolds number. In Figure 4, we have calculated manually the length of these vortices and it is also clear that
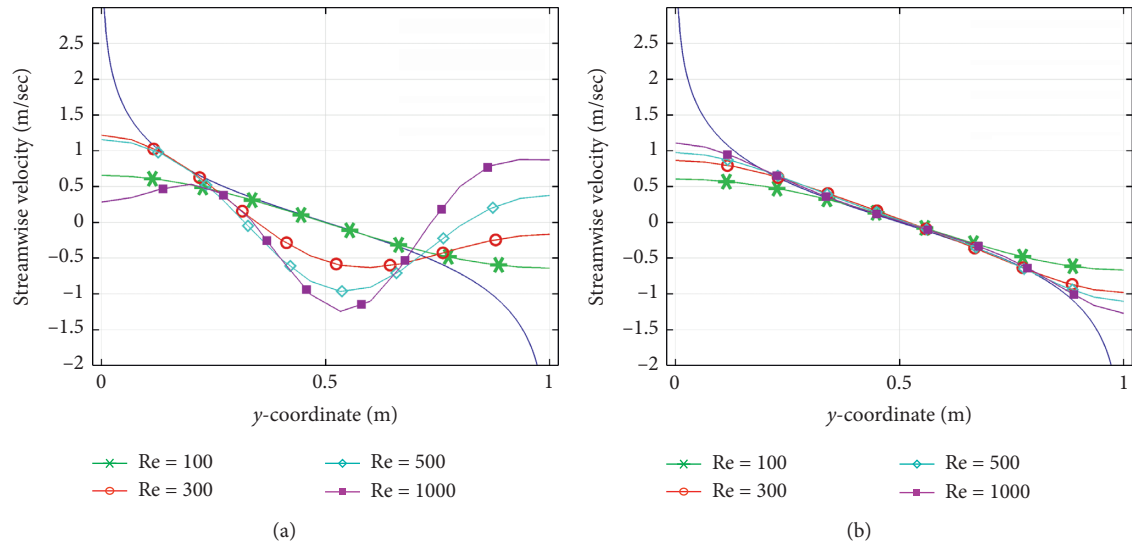
FIGURE 3: Comparison with the velocity at the stream. (a) With semicylinder and screen condition. (b) Without semicircular cylinder and screen condition.
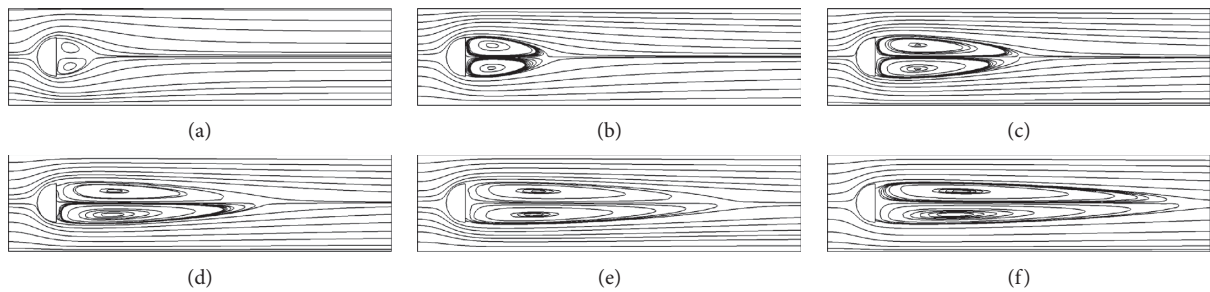
FIGURE 4: Streamlines of the velocity field at (a) Re = 100, (b) Re = 300, (c) Re = 600, (d) Re = 900, (e) Re = 1200, and (f) Re = 1500.

the lengths of these vortices are not growing equally, for example, the length of the secondary vortex is growing faster after Re = 750 when to compare with the primary vortex. From Figure 4, we are seeing that lengths of these vortices are approximately linearly related with the Reynolds number. Therefore, we apply the linear regression process to find the empirical equations given by

$$
\begin{aligned}
\mathrm{PV}_L &= 0.00177\mathrm{Re} + 0.21077, \quad 100 \leq \mathrm{Re} \leq 1500, \\
\mathrm{SV}_L &= 0.00205\mathrm{Re} + 0.18963, \quad 100 \leq \mathrm{Re} \leq 1500,
\end{aligned}
\tag{12}
$$

where $\mathrm{PV}_L$ and $\mathrm{SV}_L$ are the primary and secondary vortices, respectively.

### 2.2. Observations and Orientation of the Velocity Field.
The motive of this article, to explain the recirculating structure and the dynamics of the problem when the laminar and Newtonian fluid flow is entering the channel, is constructed by two parallel plates and a semicircle. In the session, we have to explain the orientation of the velocity field; for this purpose, we have drawn three lines L1, L2, and L3. These three lines are passing through the vortices.

L1 and L2 are the lines that are passing through the center of primary and secondary vortices, respectively, and L3 is the line passing between the vortices. The orientation of the air velocity field at the lines L1 and L3 are described in Figure 5. From Figure 6 at Re = 100, the flow rate starts at 0.0004 m/sec, then comes down to zero, and then increases rapidly above. Also, at Re = 600, it can be seen that the fluid's velocity starts normally 0.0002 m/sec, then moves a parabolic path, reaches the zero flow rate of the fluid, and then increases rapidly.

The same pattern can be seen for Re = 300, 900, 1200, and 1500 in Figure 6. The location where the speed of the fluid will become zero is the location where the center of the vortices is lying. It also can be shown from Figure 6 that the velocity of the fluid in the lines L1 and L2 shows the same pattern because these are the lines that are passing through the center of the vortices. It was also discussed that, after Re = 600, the secondary vortex is a little bit greater than the primary vortex; hence, we can see in Figure 6 for Re 1200 and 1500 that the fluid velocity has more parabolic fluctuation than in line L1.

In Figure 7, the velocity field orientation is presented at the line L3 which is passing between the vortices. At Re = 300–1500, we see that the velocity field is moving in a parabolic way up to the full length of the vortex and reaches at zero flow rate and then the fluid will become faster. We
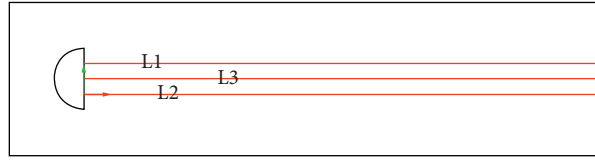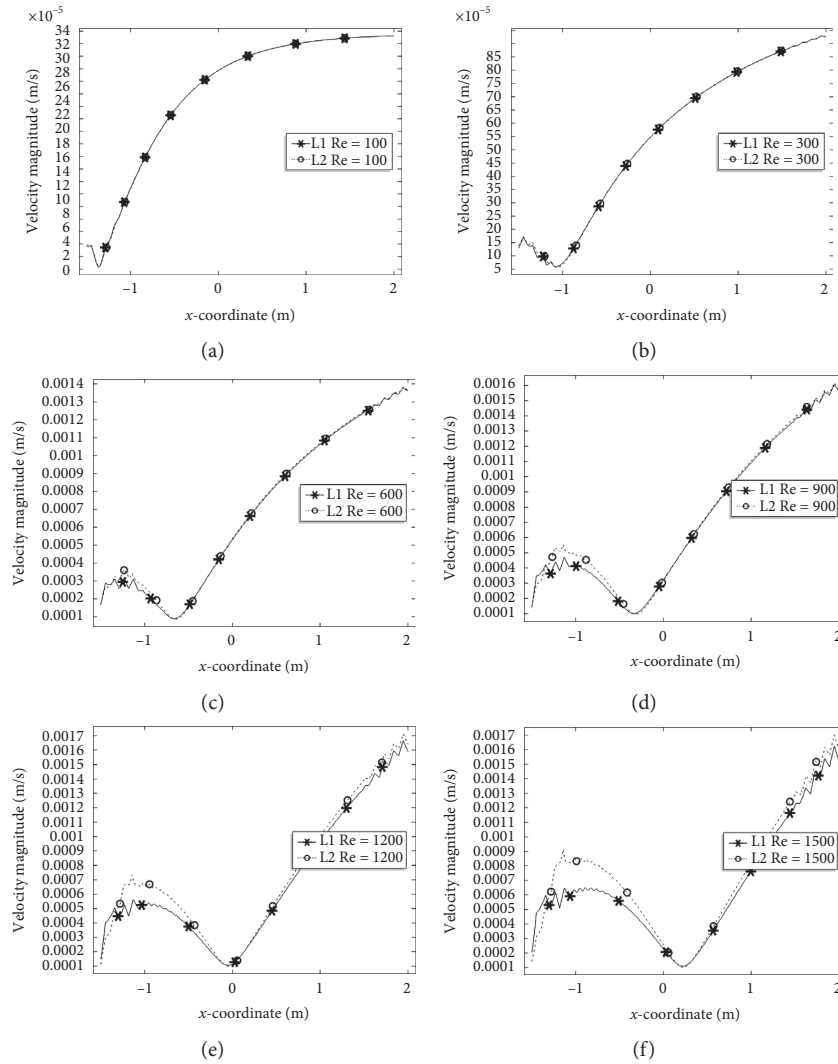
FIGURE 5: View of horizontal lines.



(a)

(b)

(c)

(d)

(e)

(f)

FIGURE 6: Orientation of the velocity field in Lines L1 and L2.

can get another advantage from Figure 7 that we can esti-mate the vortex length from the tracing of the parabolic path.

To trace the orientation of the velocity field through the $y$-axis, it is expressed by drawing the four vertical lines in the region of the vortices, as shown in Figure 8. In Figure 9 at Re = 100, we see that, as we go forward to the center the vortex, the flow rate is decreasing for all Reynolds number. Also, with the enhancement of the Reynolds number, these differences in the flow rates are declined as we see in Figure 9

for Re = 900, 1200, and 1500. We call this an *M*-shaped movement along with the vortex.

*2.3. Orientation of the Pressure along Horizontal and Vertical Lines.* It seems from Figure 10 that the pressure exerted in the recirculating region is the same horizontal for the line 1 and line 2 for all Reynolds numbers. At Re = 100, we can see that the minimum pressure is $-18e - 18$, and it is increasing
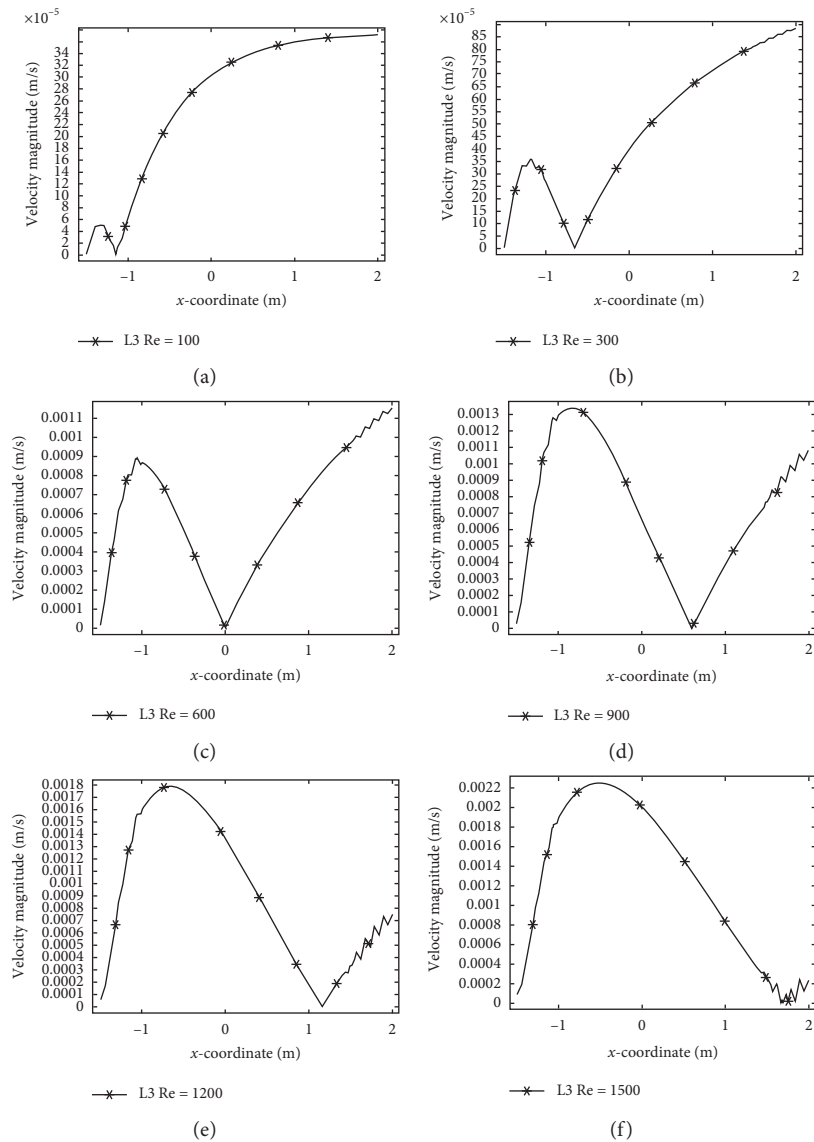
(a)

(b)

(c)

(d)

(e)

(f)

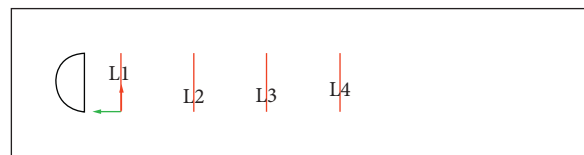FIGURE 7: Orientation of the velocity field in Lines L3.



FIGURE 8: View of vertical lines.

in line 1 and line 2. By enhancing the Reynolds number, the length of the vortex is increasing; however, it seems from Figure 10 that the growth of vortex length does not impact the pressure in the vortex region as in the case of the flow rate of the fluid.

Moreover, when to expect the pressure along the line 3, which is between line 1 and line 2, is shown in Figure 11 and has the same behavior as in line 1 and 2, and also it is increasing in the same manner. The pressure along the

recirculating region is enhanced with the enhancing of Re from 100 to 1500 and is negative which means that most of the fluid is attracted by the region. To observe the pressure along the line 3 which is between the two vortices, we see that it is not much different than when at the pressure along the line 1 and 2 except at Re = 1200.

To explain the pressure along the recirculating region, four vertical lines are drawn through the recirculating region. As we can be see in Figure 12, the pressure is increasing
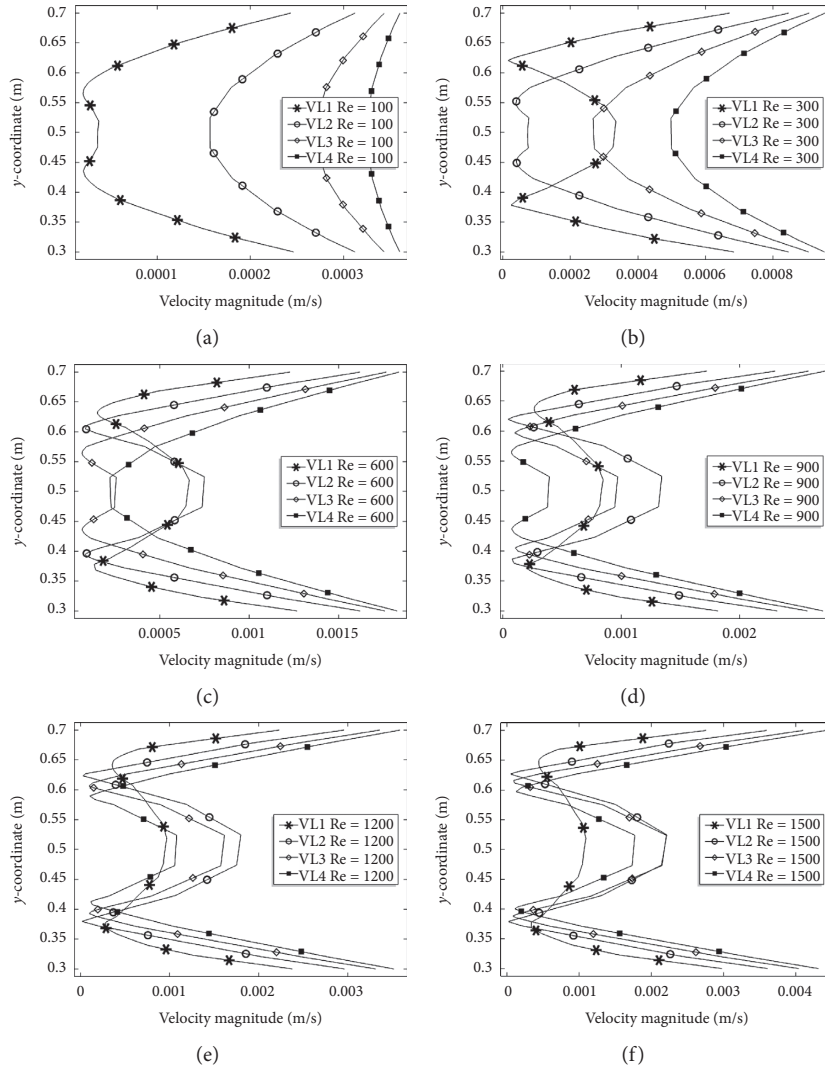
(a)

(b)

(c)

(d)

(e)

(f)

FIGURE 9: View of the velocity field along vertical lines.



(a)

(b)
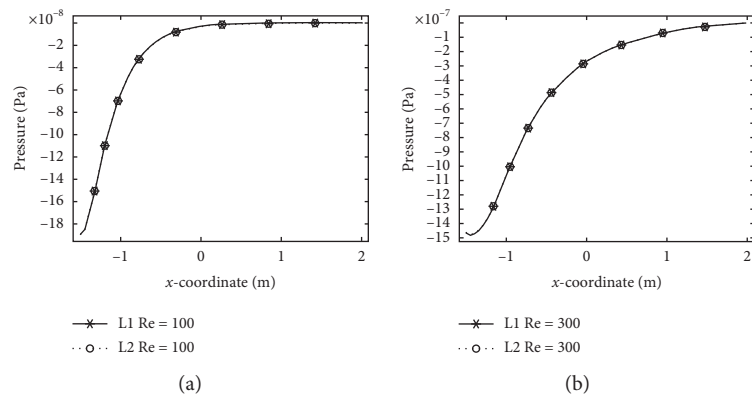
FIGURE 10: Continued.

(c)

(d)



(e)

(f)
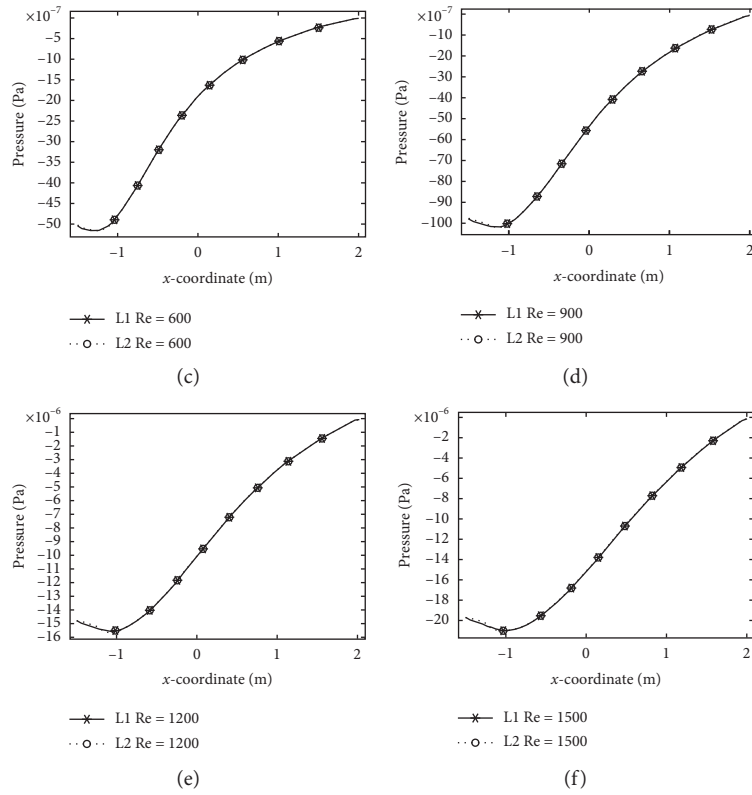
Figure 10: Pressure in lines L1 and L2.



(a)

(b)



(c)

(d)
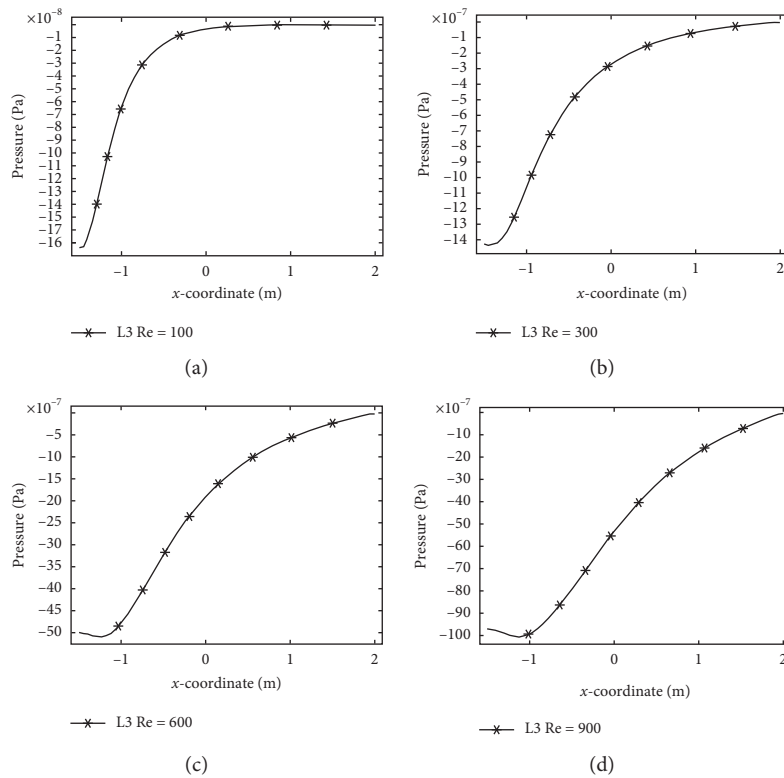
Figure 11: Continued.

(e)

(f)

FIGURE 11: Pressure along line L3.



(a)

(b)

(c)

(d)

(e)

(f)
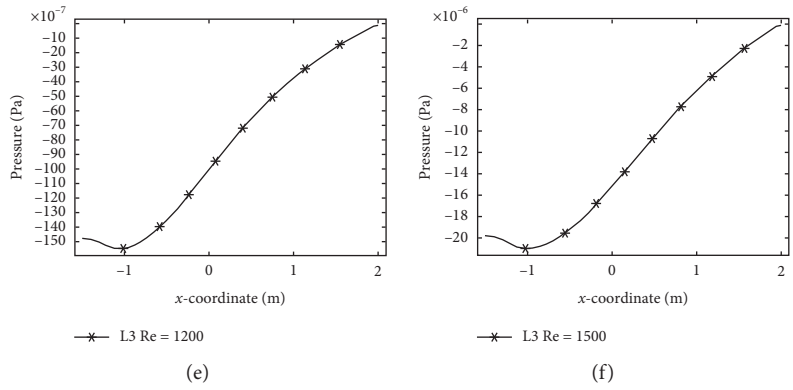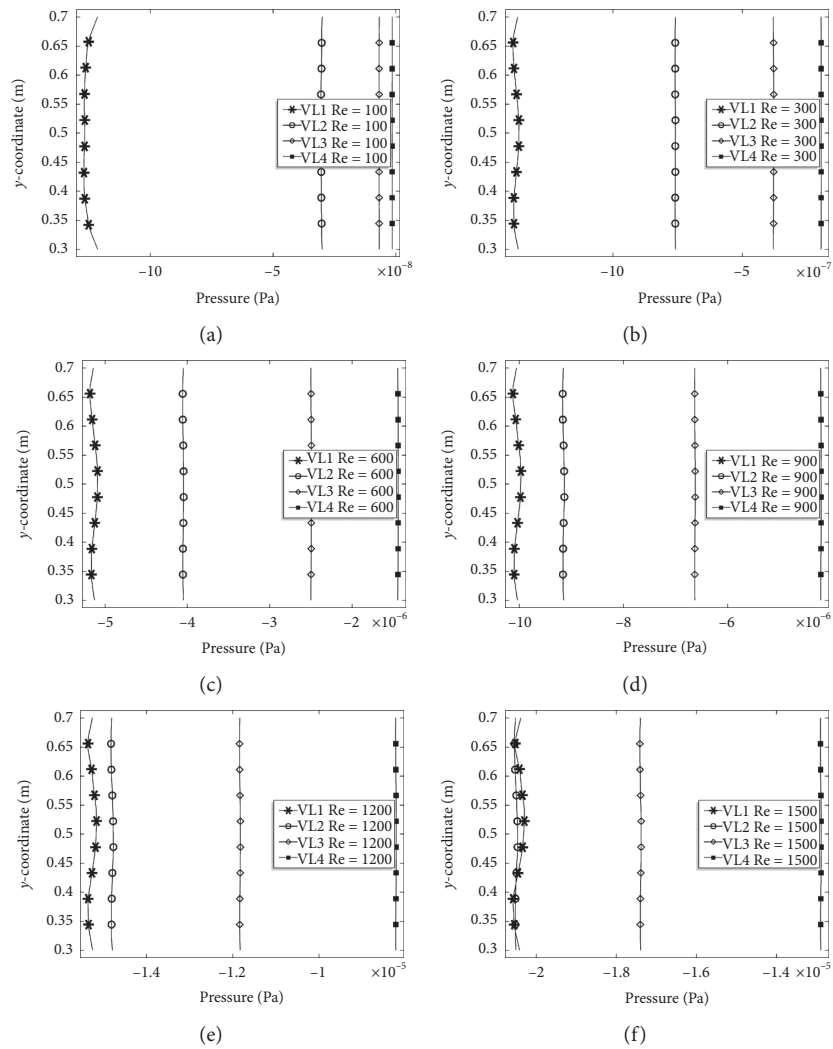
FIGURE 12: Pressure along vertical lines.

along the lines for all Reynolds number. Moreover, as we move forward to the center of the vortex, the pressure is decreasing but that difference is not fixed for all Res. As we see, the computation results for Re = 1500, where the vertical lines L1 and L2 exert the same pressure about zero difference.

## 3. Conclusion

Applying the finite element method, the Newtonian, laminar, steady-state, and incompressible fluid flow has been observed through the semicircular cylinder. The governing partial differential equation of Navier–Stokes and continuity equations were discretized and simulation was carried by emerging technology COMSOL multiphysics 5.4. An extra fine meshing was made to achieve convergence and ensure the validity by comparing the streamwise velocity obtained under screen boundary condition without semicircular cylinder and that of with semicircular cylinder under screen boundary condition. The results show a good agreement with the asymptotic solution. Furthermore, the velocity field orientation and the pressure along the recirculating region are described. The vortex lengths of the primary as well as secondary vortex formed along the boundary of semicircular cylinder were discussed in terms of the Reynolds number. We found that the vortex lengths of both vortices are increasing with enhancing the Reynolds number. The sizes of these two were different for all particular Reynolds number. Velocity magnitude of the flow through the center-line of the vortices follows the parabolic path up to the center of the vortex, becomes zero, and then increases up to the outlet of the channel for each Reynolds number. Also, for each Reynolds number, the orientation of the flow rate between the two vortices follows a parabolic path up to the full length of the vortex and then increases up to the outlet of the channel. By observing the fluid velocity on four vertical lines, it is observed that the fluid's velocity is maximum at the corner of the vortices for all Reynolds numbers. The pressure exerted by the fluid on the paths oriented through the center of the vortex is increasing up to the outlet. Also, through the path in between vortices, the pressure remains the same and increasing in the same pattern as in lines 1 and 2 through the vortices except for the result at Re = 1200. In the vortex region, the pressure along the four vertical lines was also declared and the pressure along these lines is fixed at decreasing at a comparable level as we move towards the outlet of the rectangular region. This difference will be ignored as we increase the Reynolds number.

## Data Availability

The data used to support the findings of the study are available from the corresponding author upon request.

## Conflicts of Interest

The authors declare that they have no conflicts of interest.

## Acknowledgments

## References

[1] S. Rashidi, M. Bovand, and J. Abolfazli Esfahani, "Application of magnetohydrodynamics for suppressing the fluctuations in the unsteady flow around two side-by-side circular obstacles," *The European Physical Journal Plus*, vol. 131, no. 12, p. 423, 2016.

[2] F. Hammami, B. Souayeh, N. Ben-Cheikh, and B. Ben-Beya, "Computational analysis of fluid flow due to a two-sided lid driven cavity with a circular cylinder," *Computers & Fluids*, vol. 156, pp. 317–328, 2017.

[3] R. Golani and A. Dhiman, "Fluid flow and heat transfer across a circular cylinder in the unsteady flow regime," *International Journal of Engineering and Science*, vol. 3, no. 3, pp. 8–19, 2004.

[4] G. Hauke and T. J. R. Hughes, "A unified approach to compressible and incompressible flows," *Computer Methods in Applied Mechanics and Engineering*, vol. 113, no. 3-4, pp. 389–395, 1994.

[5] J. W. Elder, "Steady flow through non-uniform gauzes of arbitrary shape," *Journal of Fluid Mechanics*, vol. 5, no. 3, pp. 355–368, 1959.

[6] A. A. Memon, H. Shaikh, and A. Ali Memon, "Finite element's analysis of fluid flow through the rectangular channel with inclined screens settled at angles," in *Proceedings of the 2019 2nd International Conference on Computing, Mathematics and Engineering Technologies (iCoMET)*, pp. 1–5, IEEE, Sukkur, Pakistan, January 2019.

[7] A. A. Memon, "Analysis of optimum velocity and pressure of the air flow through the screens with the help of resistance coefficient," *Sukkur IBA Journal of Computing and Mathematical Sciences*, vol. 3, no. 1, pp. 51–57, 2019.

[8] X. Zhang, H. Huang, Y. Zhang, and H. Wang, "Influence of a magnetic obstacle on forced convection in a three-dimensional duct with a circular cylinder," *Journal of Heat Transfer*, vol. 138, no. 1, Article ID 011703, 2016.

[9] G. B. Tezel, K. Yapici, and Y. Uludag, "Flow characterization of viscoelastic fluids around square obstacle," *Periodica Polytechnica Chemical Engineering*, vol. 63, no. 1, pp. 246–257, 2019.

[10] A. Kumar, A. Dhiman, and L. Baranyi, "CFD analysis of power-law fluid flow and heat transfer around a confined semi-circular cylinder," *International Journal of Heat and Mass Transfer*, vol. 82, pp. 159–169, 2015.

[11] C. A. Klettner, I. Eames, and J. C. R. Hunt, "The effect of an unsteady flow incident on an array of circular cylinders," *Journal of Fluid Mechanics*, vol. 872, pp. 560–593, 2019.

[12] J. Dutta and B. Kundu, "Finite integral transform based solution of second grade fluid flow between two parallel plates," *Journal of Applied and Computational Mechanics*, vol. 5, no. 5, pp. 989–997, 2019.

[13] A. Rauf, "An analytical and semi-analytical study of the oscillating flow of generalized burgers' fluid through a circular porous medium," *Journal of Applied and Computational Mechanics*, vol. 5, no. 5, pp. 827–839, 2019.

[14] M. Fomicheva, W. H. Müller, E. N. Vilchevskaya, and N. Bessonov, "Funnel flow of a Navier-Stokes-fluid with potential applications to micropolar media," *Facta*

*Universitatis, Series: Mechanical Engineering*, vol. 17, no. 2, pp. 255–267, 2019.

[15] O. Bazighifan and H. Ramos, "On the asymptotic and oscillatory behavior of the solutions of a class of higher-order differential equations with middle term," *Applied Mathematics Letters*, vol. 107, Article ID 106431, 2020.

[16] O. Bazighifan, "Kamenev and Philos-types oscillation criteria for fourth-order neutral differential equations," *Advances in Difference Equations*, vol. 2020, no. 1, pp. 1–12, 2020.